Journal of Thermal Analysis and Calorimetry (2023) 148:1679–1686
https://doi.org/10.1007/s10973-022-11728-3

Determination of the activation energy under isothermal conditions: revisited

Juan Arcenegui-Troya[1] · Pedro Enrique Sánchez-Jiménez[1,2] · Antonio Perejón[1,2] · Luis Allan Pérez-Maqueda[1]

Received: 25 February 2022 / Accepted: 17 October 2022 / Published online: 11 November 2022

Abstract
The kinetic analysis of solid-state processes aims at obtaining fundamental information that can be used for predicting the time evolution of a process within a wide range of conditions. It is an extended belief that the determination of the kinetic parameters from the analysis of curves recorded under isothermal conditions is strongly conditioned by the kinetic model used to fit the experimental data. Thus, much effort is devoted to finding the model that truly describes a process in order to calculate the kinetic parameters with accuracy. In this work, we demonstrate that the value of activation energy determined from kinetic analysis of isothermal curves is independent of the kinetic model used to fit the experimental data and, taking advantage of the underlying reason for this, a method for determining the activation energy with two isothermal curves is proposed.

Keywords Kinetic · Isothermal · Activation energy · Model-free · Solid-state process

Introduction

The kinetic analysis of solid-state processes allows obtaining fundamental information that can be used for modelling a myriad of processes with direct application to industry [1–11]. Kinetic analysis is quite challenging not only in terms of obtaining reliable experimental data [12–14], but also from the point of view of extracting the kinetic parameters from these experimental curves [9, 15]. The main purpose of a kinetic analysis is to determine the kinetic parameters that describe the process and allow predicting its thermal behaviour with accuracy in a wide range of conditions, usually different from those used for the analysis. Recently, it has been recognized that predictions are compromised if the selection of the kinetic model is not properly performed [16]. Moreover, ideal kinetic models in the literature have been proposed assuming ideal conditions that are rare in real systems that present intrinsic features. For example, these ideal models assume homogeneous materials in terms of particle size, while ideal samples usually present a broad particle size distribution (PSD). Previous studies have shown that the PSD might influence the results of kinetic analysis [17]. For instance, it has been demonstrated that interface reaction models can be confused with diffusion or nucleation models if the PSD is not taken into account [18].

The experimental data used in the kinetic analysis can be recorded under a wide range of conditions and using different thermal analysis techniques, including differential scanning calorimetry (DSC), thermogravimetric analysis (TGA) and high-temperature X-ray diffraction. The experimental conditions are often limited by the process studied and the method employed. Concerning this, the isothermal kinetic analysis presents certain advantages as compared to other conditions employed to study solid-state processes. For instance, kinetic studies conducted under isothermal conditions are more effective when discriminating the kinetic model as compared to other approaches, since the shape of the extent of conversion versus time curves directly reflects the kinetic model obeyed by a process [19]. The isothermal kinetic analysis continues to be amply employed nowadays to study a wide range of processes. Thus, it is

✉ Juan Arcenegui-Troya
jjarcenegui@icmse.csic.es

✉ Luis Allan Pérez-Maqueda
maqueda@cica.es

[1] Instituto de Ciencia de Materiales de Sevilla, C.S.I.C.-Universidad de Sevilla, C. Américo Vespucio No. 49, 41092 Seville, Spain

[2] Departamento de Química Inorgánica, Facultad de Química, Universidad de Sevilla, 41012 Seville, Spain

the most feasible option for reactions studied under realistic conditions of operation [19, 20], long-term curing [21, 22], oxidation and reduction processes [23, 24], hydration and dehydration processes [25–27], reactions followed through X-ray diffraction [28] or those studies intended to discriminate the kinetic model under isothermal conditions [29–32].

Here, we demonstrate mathematically that the value of activation energy determined from kinetic analysis of isothermal curves is independent of the selected model used to fit the data. To the best of our knowledge, this demonstration is unprecedented and has significant implications, as reported values of activation energy are valid independently of the assumed kinetic model. Furthermore, taking advantage of some of the mathematical arguments that led to that conclusion, we present a simple methodology to obtain the values of the activation energy through analysis of two curves recorded under isothermal conditions. The method is validated by analysing different experimental curves, corresponding to different processes, namely the thermal degradation of ethylene–propylene–diene, the thermal decomposition of limestone and the cure of a clear laminating epoxy resin, and comparing the results with those reported in the literature.

Theoretical foundation

The equation that describes the rate of solid-state processes is [7]:

$$\frac{\mathrm{d}\alpha}{\mathrm{d}t} = k(T)f(\alpha) \tag{1}$$

where t is the time, α is the extent of conversion, $f(\alpha)$ is the kinetic model, and $k(T)$ is the Arrhenius function given by:

$$k(T) = A\exp\left(-\frac{E_\mathrm{a}}{RT}\right) \tag{2}$$

Being A a pre-exponential factor, E_a the activation energy, R the gas constant and T the temperature. In isothermal conditions, $k(T)$ becomes a constant and Eq. 1 can be integrated as follows:

$$\int_0^\alpha \frac{\mathrm{d}\alpha}{f(\alpha)} = k\int_0^t \mathrm{d}t \rightarrow g(\alpha) = kt \tag{3}$$

where $g(\alpha) = \int_0^\alpha \mathrm{d}\alpha/f(\alpha)$ is the integral form of the kinetic model. Let us consider a process studied under isothermal conditions at two different temperatures, T_1 and T_2. According to Eq. 2, different values of the rate constant k will be obtained, so that:

$$\left.\frac{\mathrm{d}\alpha}{\mathrm{d}t}\right|_{T_1} = k_1 f(\alpha) \tag{4a}$$

$$\left.\frac{\mathrm{d}\alpha}{\mathrm{d}t}\right|_{T_2} = k_2 f(\alpha) \tag{4b}$$

Therefore:

$$\left.\frac{\mathrm{d}\alpha}{\mathrm{d}t}\right|_{T_2} = k_2 f(\alpha) = \frac{k_2}{k_1} k_1 f(\alpha) = \frac{k_2}{k_1}\left.\frac{\mathrm{d}\alpha}{\mathrm{d}t}\right|_{T_1} \tag{5}$$

From this equation, we can derive the relationship between the time invested in reaching a given value of α in the two isothermal experiments.

$$\mathrm{d}t|_{T_2} = \frac{k_1}{k_2}\mathrm{d}t|_{T_1} \rightarrow \int \mathrm{d}t|_{T_2} = \frac{k_1}{k_2}\int \mathrm{d}t|_{T_1} \rightarrow t|_{T_2} = \frac{k_1}{k_2}t|_{T_1} \tag{6}$$

Figure 1 illustrates the proportionality relationship between the times required to reach a certain value of α at two different temperatures, being the constant of proportionality equal to the ratio between the rate constants. Data shown in Fig. 1a were calculated using a Runge–Kutta method to solve Eq. 1 for $T_1 = 750$ K and $T_2 = 800$ K, assuming $f(\alpha) = 3(1-\alpha)^{2/3}$ (contracting volume model R3) [7], $E_a = 180$ kJ mol^{-1} and $A = 10^9$ s^{-1}. As might be observed in Fig. 1b, both curves overlap when the values of time corresponding to the curve calculated for T_2 are multiplied by the ratio between the two rate constants k_1/k_2.

The standard method based on the fitting to ideal models to determine the activation energy from isothermal experiments consists of recording several curves at different temperatures and representing some selected kinetic models $g(\alpha)$ as a function of t to estimate which of them best linearizes the data [7]. The process is supposed to obey the model that provides the value of the correlation coefficient closest to one, and the slope of the best-fitting line to the data is assumed to be the rate constant k. Then, the activation energy and the pre-exponential factor can be determined by plotting the logarithm of k versus $1/T$.

Let's suppose that we have a set of n isotherms recorded at different temperatures: T_1,T_2, T_3….T_n. If we represent $g(\alpha)$ as a function of t for an arbitrary given model and apply the linear least squares approximation, the slope for the isotherm corresponding to T_i is given by:

$$s_i = \frac{N\sum_{j=1}^{N} g(\alpha_j)\, t_j\big|_{T_i} - \sum_{j=1}^{N} g(\alpha_j)\sum_{j=1}^{N} t_j\big|_{T_i}}{N\sum_{j=1}^{N}\left(t_j\big|_{T_i}\right)^2 - \left(\sum_{j=1}^{N} t_j\big|_{T_i}\right)^2} \tag{7}$$

Being N the number of points (t, α) recorded during the experiment. According to Eq. 6, each value $t_j\big|_{T_i}$ is related to $t_j\big|_{T_1}$ through the following equation:

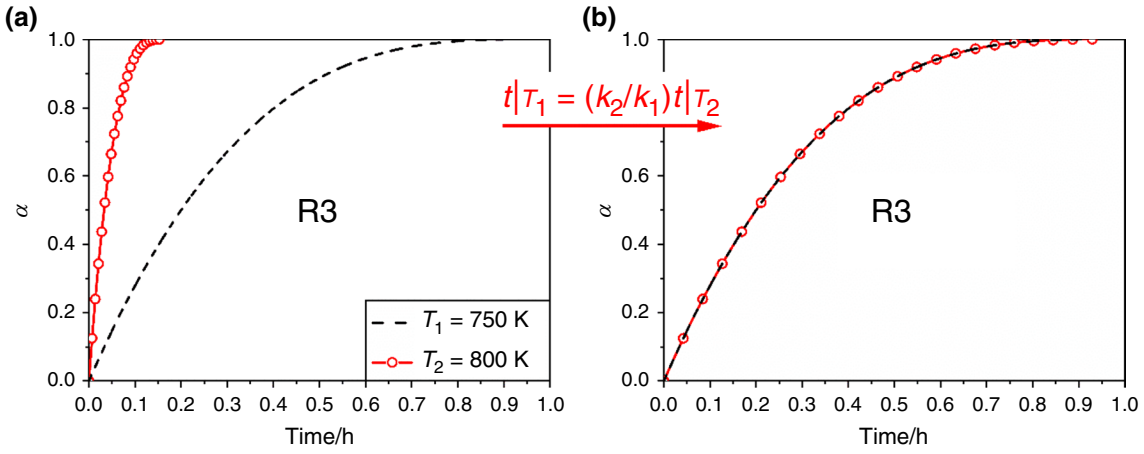

Fig. 1 **a** Curves simulated assuming a contracting volume model and isothermal conditions with $T_1 = 750$ K and $T_2 = 800$ K, $E_a = 180$ kJ mol^{-1} and $A = 10^9$ s^{-1}. **b** Overlapping of both curves when the values of time calculated for T_2 are multiplied by k_2/k_1

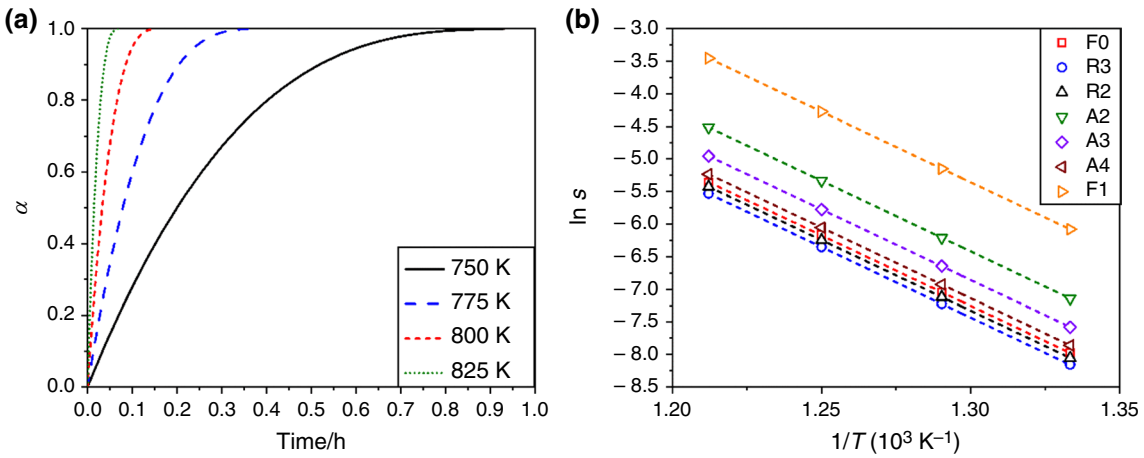

Fig. 2 **a** Curves simulated assuming a contracting volume model (R3) and isothermal conditions: 750 K, 775 K, 800 K and 825 K. $E_a = 180$ kJ mol^{-1} and $A = 10^9$ s^{-1}. **b** $\ln s$ as a function of $1/T$ for different ideal kinetic models

$$t_j\Big|_{T_i} = \frac{k_1}{k_i}\, t_j\Big|_1 \tag{8}$$

Substituting this into Eq. 7, we get:

$$\begin{aligned} s_i &= \frac{N\sum_{j=1}^{N} g(\alpha_j)(k_1/k_i)t_j\Big|_1 - \sum_{j=1}^{N} g(\alpha_j)\sum_{j=1}^{N}(k_1/k_i)t_j\Big|_1}{N\sum_{j=1}^{N}\left((k_1/k_i)t_j\Big|_1\right)^2 - \left(\sum_{j=1}^{N}(k_1/k_i)t_j\Big|_1\right)^2} \\ &= \left(\frac{k_i}{k_1}\right)\frac{N\sum_{j=1}^{N} g(\alpha_j)\,t_j\Big|_1 - \sum_{j=1}^{N} g(\alpha_j)\sum_{j=1}^{N} t_j\Big|_1}{N\sum_{j=1}^{N}\left(t_j\Big|_1\right)^2 - \left(\sum_{j=1}^{N} t_j\Big|_1\right)^2} \\ &= \left(\frac{k_i}{k_1}\right)s_1 \quad \text{for} \quad i > 1 \end{aligned} \tag{9}$$

By taking logarithms, considering that $k_i = A\exp\left(-E_a/RT_i\right)$, and rearranging terms it follows:

$$\ln s_i = \ln\left(\frac{s_1}{k_1}\right) - \frac{E_a}{RT_i} + \ln A \quad \text{for} \quad i > 1 \tag{10}$$

Thus, regardless of the kinetic model used, s_i linearly depends only on $1/T_i$ with slope $-E_a/R$. Equivalently, the activation energy determined by this approach will be the same for any kinetic model employed. Note that when the kinetic model actually obeyed is selected, $s_1 = k_1$ and Eq. 10 becomes:

$$\ln k_i = -\frac{E_a}{RT_i} + \ln A \tag{11}$$

Thus, the activation energy can be determined from the slope and the pre-exponential factor from the intercept of

Table 1 Values of activation energy, rate constants and correlation coefficients obtained from fitting the data plotted in Fig. 2a to Eq. 3 assuming different kinetic models

Kinetic model	750 K		775 K		800 K		825 K		E_a/kJ mol^{-1}
	s/s^{-1}	R^2	S/s^{-1}	R^2	s/s^{-1}	R^2	s/s^{-1}	R^2	
F0	0.00034	0.8355	0.00087	0.8355	0.00209	0.8355	0.00474	0.8355	180
F1	0.00229	0.7923	0.00581	0.7923	0.01391	0.7923	0.03160	0.7923	180
R2	0.00032	0.9752	0.00081	0.9752	0.00194	0.9752	0.00440	0.9752	180
R3	0.00029	1	0.00073	1	0.00174	1	0.00396	1	180
A2	0.00079	0.9687	0.00201	0.9687	0.00482	0.9687	0.01094	0.9687	180
A3	0.00051	0.9354	0.00130	0.9354	0.00310	0.9354	0.00705	0.9354	180
A4	0.00039	0.8720	0.00098	0.8720	0.00235	0.8720	0.00534	0.8720	180

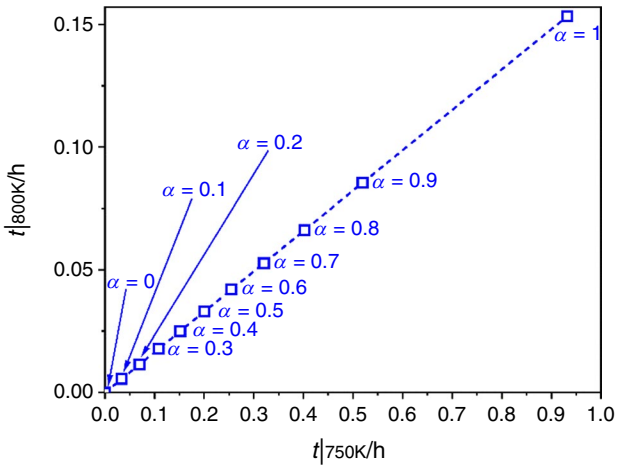

Fig. 3 Values of $t|_{800K}$ as a function of $t|_{750K}$ for different values of the extent of conversion

the line logarithm of k versus $1/T$. Figure 2a shows the extent of conversion as a function of time for four temperatures: 750 K, 775 K, 800 K and 825 K. Data were simulated assuming isothermal conditions, the kinetic model R3, E_a =180 kJ mol^{-1} and $A=10^9$ s^{-1}. Table 1 collects the results obtained from fitting these data to Eq. 3 assuming different kinetic models. As expected, the value of the correlation coefficient obtained is maximum for the kinetic model R3. This analysis illustrates that the value of the activation energy does not depend on the kinetic model assumed; the slope of the line $\ln s$ versus $1/T$ is the same for all the kinetic models studied, consistently with Eq. 10.

The relationship expressed by Eq. 6 enables us to develop a simple method for determining the activation energy with two curves recorded under isothermal conditions, which significantly simplify the typical procedure. Indeed, by plotting the time required to attain a certain value of the extent of conversion at T_2 against the time needed when the isotherm is conducted at T_1, we obtain a line which slope is given by $m = k_1/k_2$. Thus, taking into account Eq. 2 for the Arrhenius function, the activation energy can be calculated as:

$$E_a = R\frac{T_1 \cdot T_2}{(T_1 - T_2)} \ln m \tag{12}$$

Let us apply this method to data plotted in Fig. 1. Figure 3 shows the values of $t|_{800K}$ as a function of $t|_{750K}$ for different values of the extent of conversion. The slope of the best-fitting line is m=0.16445, and applying Eq. 12 we obtain E_a=180 kJ mol^{-1} as expected, which validate the method for determining the value of the activation energy with two of the isothermal curves shown in Fig. 2.

Experimental section

The method described in Sect. 2 was applied to the study of three different reactions: the pyrolysis of ethylene–propylene–diene (EPDM), the thermal decomposition of limestone and the curing of an epoxy resin. The sample

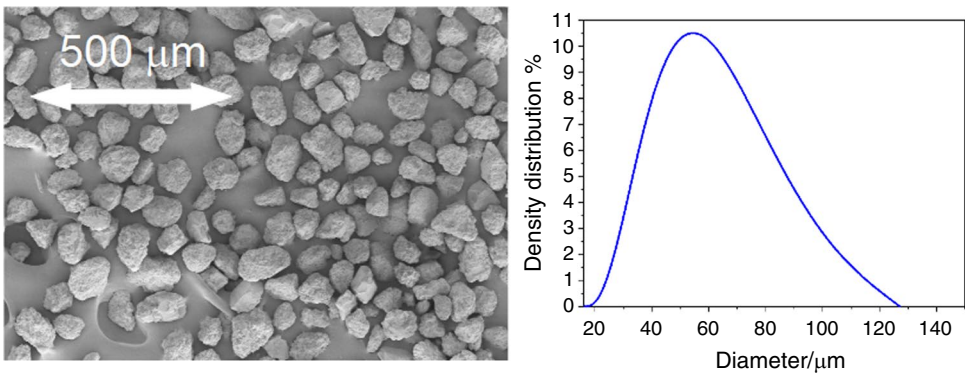

Fig. 4 SEM micrograph and particle size distribution of the sample of limestone used in this work

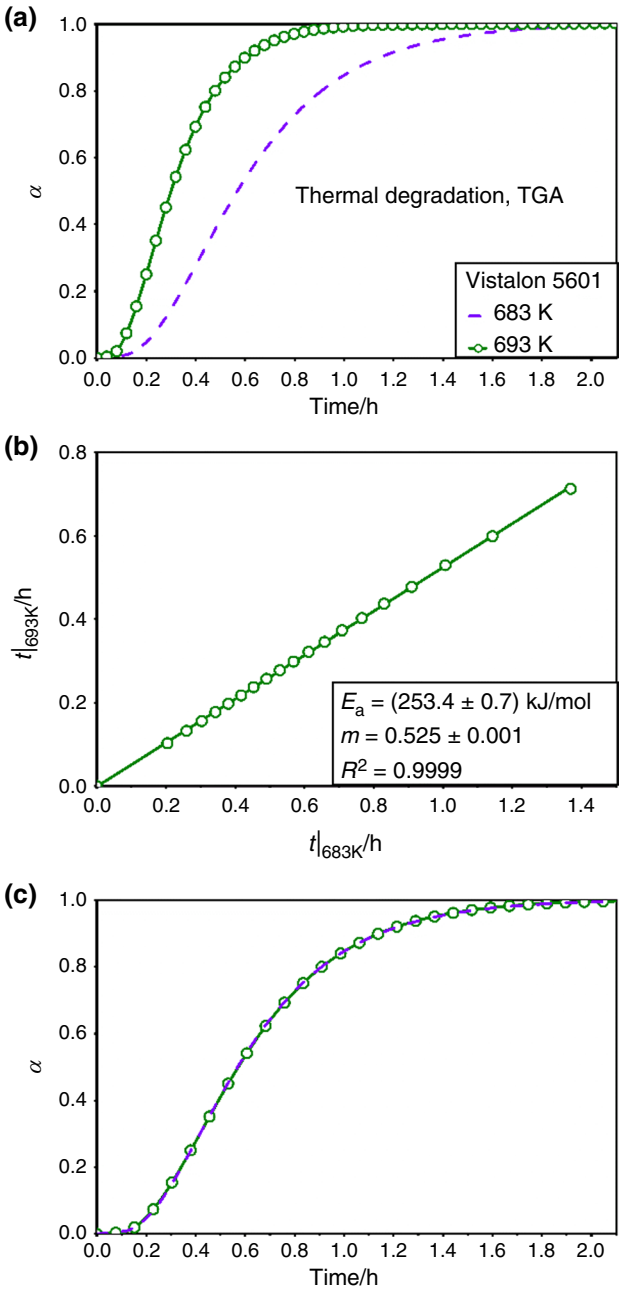

Fig. 5 **a** Curves recorded under isothermal conditions at 683 K and 693 K for the pyrolysis of EPDM. **b** Linear relationship between the values of time needed to reach a certain value of α at the two different temperatures employed. **c** Overlapping of both curves after applying Eq. 6. The value of activation energy obtained is $E_a = (253.4 \pm 0.7)$ kJ mol^{-1}

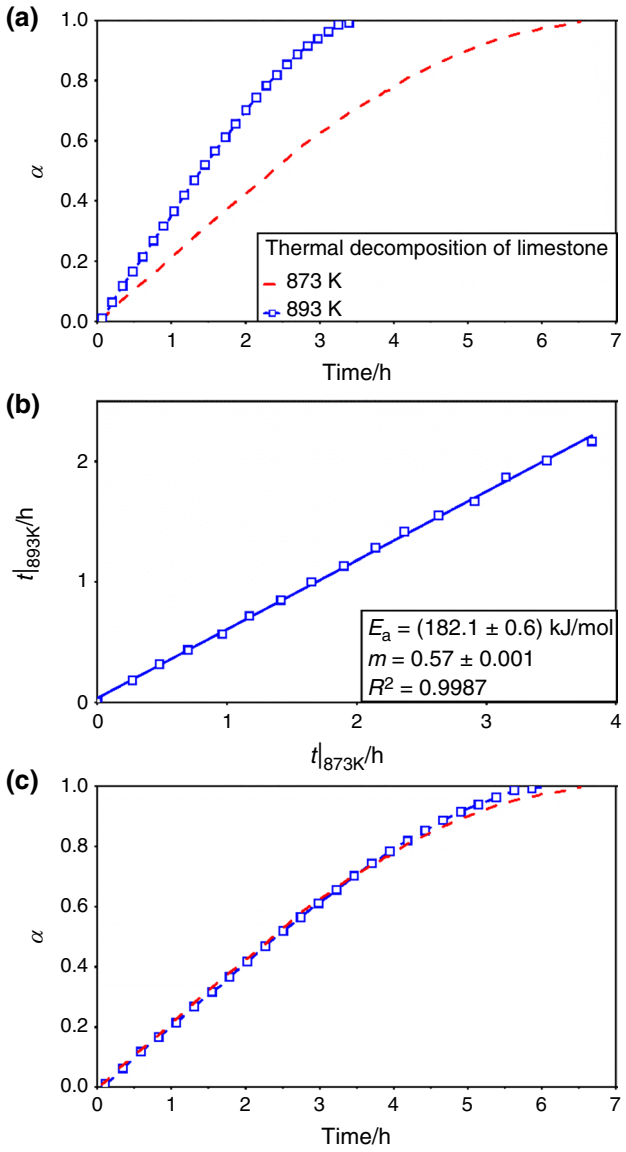

Fig. 6 **a** Time evolution of the extent of decomposition of limestone at 873 and 893 K. **b** Linear relationship between the values of time needed to reach a certain value of α at the two different temperatures employed. **c** Overlapping of both curves after applying Eq. 6. The value of activation energy obtained is $E_a = (182.1 \pm 0.6)$ kJ mol^{-1}

of (EPDM) used was supplied by ExxonMobil (Vistalon Rubbers): 69 mass% ethylene, 5 mass% ethylidene norbornene and 26 mass% propylene. The limestone (ESKAL 60) was provided by KSL Staubtechnik GmbH (Germany). Figure 4 shows a scanning electron micrograph and the particle size distribution (PSD) of the sample of limestone used. As might be observed, the sample exhibits a narrow PSD with a peak around 60 μm. Both the thermal degradation of EPDM and the decomposition of limestone were studied in isothermal conditions using a thermogravimetric analyser Q5000IR from TA instruments. The experiments started with a heating ramp at 300 °C min^{-1} from room temperature to the temperature of the isotherm. Then, the temperature was maintained constant for two hours in the experiments with EPDM and seven hours in the case of limestone. The experiments were carried out in nitrogen with a flow rate of 200 mL min^{-1}. On the other

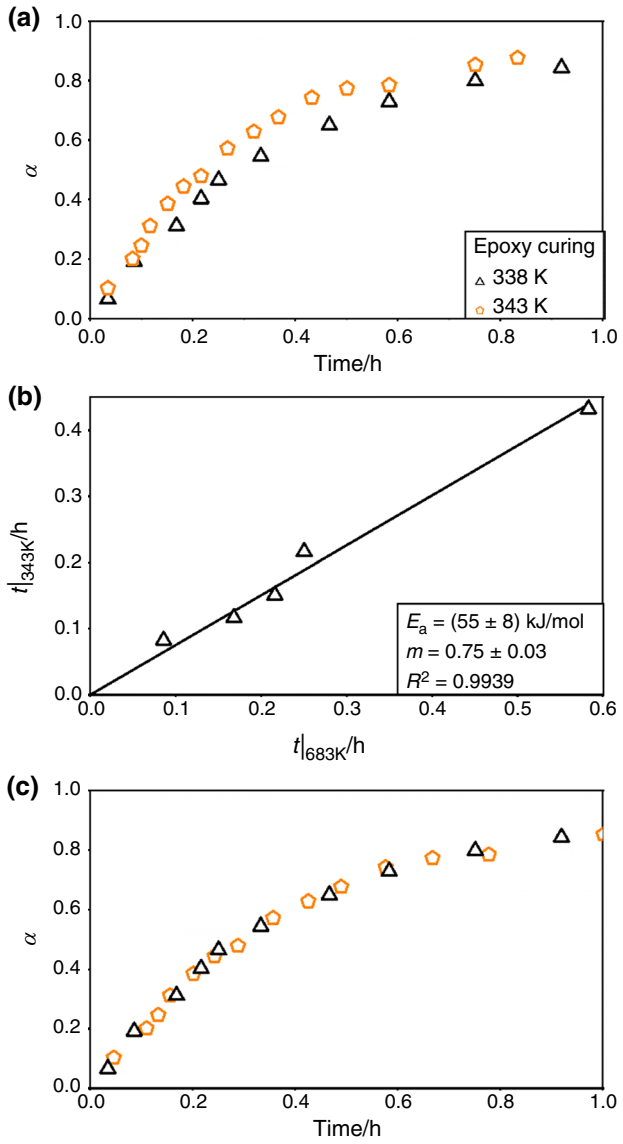

Fig. 7 **a** Degree of curing as a function of time, recorded under isothermal conditions in a DSC, at 338 K and 343 K. **b** Linear relationship between the values of time needed to reach a certain value of α at the two different temperatures employed. **c** Overlapping of both curves after applying Eq. 6

hand, the data corresponding to the curing of the epoxy resin were taken from the literature [22].

Results and discussion

Figure 5a shows the time evolution of the extent of degradation of EPDM corresponding to two isothermal experiments carried out at 683 K and 693 K. As can be observed in Fig. 5b, there is a linear relationship between the values of time needed to reach a certain value of α at the two different temperatures employed. The value of apparent activation energy calculated from the slope, after applying Eq. 12, is $E_a = (253.4 \pm 0.7)$ kJ mol^{-1}, which is in agreement with that reported in the literature $E_a = (252 \pm 8)$ kJ/mol [33]. Figure 5c illustrates that both isotherms overlap when Eq. 6 is applied using the value of E_a calculated from the slope of the line plotted in Fig. 4b.

Data corresponding to the thermal decomposition of limestone are plotted in Fig. 6. These curves were recorded at 873 K and 893 K. The value of activation energy obtained in this case is $E_a = (182.1 \pm 0.6)$ kJ mol^{-1}. This reaction has received a great deal of interest in recent years because it is in the core of the so-called "calcium looping" technology for CO_2 capture and the storage of concentrated solar power [34, 35]. Thus, the reaction has been amply studied and the values of activation energy reported in the literature are in good agreement with the one determined in this work [19, 36–38].

The same method was applied to data corresponding to experiments in which clear laminating epoxy resin curing was monitored by DSC at two distinct temperatures: 338 K and 343 K. As aforementioned, the experimental results, shown in Fig. 7a, were published by Tziamtzi et al. [22]. The value of activation energy determined using the method proposed, (55 ± 7) kJ mol^{-1}, is in agreement with the values reported in the work from which the data were obtained. Besides, it is also in line with other results previously reported in the literature for this type of material [39, 40].

The three cases analysed above served us to validate the method with data recorded under different experimental conditions, demonstrating its general applicability.

Conclusions

In this work, it has been demonstrated that the apparent activation energy calculated from isothermal analysis based on the fitting to ideal kinetic models is independent of the model selected to do the fitting. Furthermore, a method to calculate the activation energy from two isothermal experiments has been presented. The method was applied to the analysis of data corresponding to experiments conducted in a TGA, namely the pyrolysis of EPDM and the thermal decomposition of limestone. The comparison with the apparent activation energies previously reported for these reactions demonstrated the reliability of the method. Moreover, to extend its range of applicability, the method has been also validated through its application to data from the literature recorded by differential scanning calorimetry.

Acknowledgements This work has been funded by the grant CTQ2017-83602-C2-1-R (MCIN/AEI/https://doi.org/10.13039/501100011033 and ERDF A way of making Europe by the European Union), grant PDC2021-121552-C21 (MCIN/AEI/https://doi.org/10.13039/501100011033 and European Union Next GenerationEU/PRTR), projects P18-FR-1087 and US-1262507 (Junta de Andalucía-Consejería de Conocimiento, Investigación y Universidad-Fondo Europeo de Desarrollo Regional (FEDER) (Programa Operativo FEDER Andalucía 2014–2020) and INTRAMURAL-CSIC grant numbers 201960E092 and 202060I004. JAT acknowledges financial support received from Junta de Andalucía-Consejería de Economía, Conocimiento, Empresas y Universidad via a postdoctoral fellowship with reference DOC_00044.

Author contributions All authors contributed to the study conception and design. Material preparation, data collection and analysis were performed by JA-T, AP and PE. Sánchez-Jiménez. The first draft of the manuscript was written by JA-T, and all authors commented and revised previous versions of the manuscript. All authors read and approved the final manuscript. Supervision was performed by LAP-M.

Funding Open Access funding provided thanks to the CRUE-CSIC agreement with Springer Nature.

References

1. Trache D, Maggi F, Palmucci I, DeLuca LT. Thermal behavior and decomposition kinetics of composite solid propellants in the presence of amide burning rate suppressants. J Therm Anal Calorim. 2018;132:1601–15.
2. Fedunik-Hofman L, Bayon A, Donne SW. Kinetics of solid-gas reactions and their application to carbonate looping systems. Energies. 2019;12:2981.
3. Okhrimenko L, Dussouillez J, Johannes K, Kuznik F. Thermodynamic equilibrium and kinetic study of lanthanum chloride heptahydrate dehydration for thermal energy storage. J Energy Storage. 2022;48: 103562.
4. Gasparini E, Tarantino SC, Ghigna P, Riccardi MP, Cedillo-González EI, Siligardi C, et al. Thermal dehydroxylation of kaolinite under isothermal conditions. Appl Clay Sci. 2013;80–81:417–25.
5. Liu X, Liu X, Hu Y. Investigation of the thermal behaviour and decomposition kinetics of kaolinite. Clay Miner. 2015;50:199–209.
6. Taibi A, Chaguetmi S, Louaer A, Layachi A, Satha H. Barium calcium titanate solid solution: non-isothermal kinetic analysis of Ca^{2+} incorporation into $BaTiO_3$. Thermochim Acta. 2019;680: 178356.
7. Khawam A, Flanagan DR. Solid-state kinetic models: basics and mathematical fundamentals. J Phys Chem B. 2006;110:17315–28.
8. Perejón A, Sánchez-Jiménez PE, Criado JM, Pérez-Maqueda LA. Kinetic analysis of complex solid-state reactions: a new deconvolution procedure. J Phys Chem B. 2011;115:1780–91.
9. Vyazovkin S, Burnham AK, Favergeon L, Koga N, Moukhina E, Pérez-Maqueda LA, et al. ICTAC kinetics committee recommendations for analysis of multi-step kinetics. Thermochim Acta. 2020;689: 178597.
10. Wan P, Zhou J, Li Y, Yin Y, Peng X, Ji X, et al. Kinetic analysis of resin binder for casting in combustion decomposition process. J Therm Anal Calorim. 2021. https://doi.org/10.1007/s10973-021-10902-3.
11. Málek J, Svoboda R. Kinetic processes in amorphous materials revealed by thermal analysis: application to glassy selenium. Molecules. 2019;24:2775.
12. Wang Y, Tan S, Bell DA. Steam gasification of powder river basin coal: surface reaction kinetics and intraparticle mass transfer restrictions. J Therm Anal Calorim. 2021;146:2209–22.
13. Arcenegui-Troya J, Durán-Martín JD, Perejón A, Valverde JM, Pérez Maqueda LA, Sánchez Jiménez PE. Overlooked pitfalls in CaO carbonation kinetics studies nearby equilibrium: Instrumental effects on calculated kinetic rate constants. Alexandria Eng J. 2022;61:6129–38.
14. Vyazovkin S, Chrissafis K, Di Lorenzo ML, Koga N, Pijolat M, Roduit B, et al. ICTAC kinetics committee recommendations for collecting experimental thermal analysis data for kinetic computations. Thermochim Acta. 2014;590:1–23.
15. Vyazovkin S, Burnham AK, Criado JM, Pérez-Maqueda LA, Popescu C, Sbirrazzuoli N. ICTAC kinetics committee recommendations for performing kinetic computations on thermal analysis data. Thermochim Acta. 2011;520:1–19.
16. Sánchez-Jiménez PE, Perejón A, Arcenegui-Troya J, Pérez-Maqueda LA. Predictions of polymer thermal degradation: relevance of selecting the proper kinetic model. J Therm Anal Calorim. 2021;147:2335–41.
17. Koga N, Criado JM. Kinetic analyses of solid-state reactions with a particle-size distribution. J Am Ceram Soc. 1998;81:2901–9.
18. Arcenegui-Troya J, Sánchez-Jiménez PE, Perejón A, Pérez-Maqueda LA. Relevance of particle size distribution to kinetic analysis: the case of thermal dehydroxylation of kaolinite. Processes. 2021;9:1852.
19. Arcenegui-Troya J, Sánchez-Jiménez PE, Perejón A, Moreno V, Valverde JM, Pérez-Maqueda LA. Kinetics and cyclability of limestone ($CaCO_3$) in presence of steam during calcination in the CaL scheme for thermochemical energy storage. Chem Eng J. 2021;417: 129194.
20. Ortiz C, Valverde JM, Chacartegui R, Perez-Maqueda LA. Carbonation of limestone derived CaO for thermochemical energy storage: from kinetics to process integration in concentrating solar plants. ACS Sustain Chem Eng. 2018;6:6464–6417.
21. Hu J, Shan J, Zhao J, Tong Z. Isothermal curing kinetics of a flame retardant epoxy resin containing DOPO investigated by DSC and rheology. Thermochim Acta. 2016;632:56–63.
22. Tziamtzi CK, Chrissafis K. Optimization of a commercial epoxy curing cycle via DSC data kinetics modelling and TTT plot construction. Polymer. 2021;230:124091.
23. Huo J, Zhao S, Pan J, Pu W, Varfolomeev MA, Emelianov DA. Evolution of mass losses and evolved gases of crude oil and its SARA components during low-temperature oxidation by isothermal TG–FTIR analyses. J Therm Anal Calorim. 2022;147:4099–112.
24. Wang G, Min X, Peng N, Wang Z. The isothermal kinetics of zinc ferrite reduction with carbon monoxide. J Therm Anal Calorim. 2021;146:2253–60.
25. Kodani S, Iwasaki S, Favergeon L, Koga N. Revealing the effect of water vapor pressure on the kinetics of thermal

decomposition of magnesium hydroxide. Phys Chem Chem Phys. 2020;22:13637–49.
26. Koga N, Favergeon L, Kodani S. Impact of atmospheric water vapor on the thermal decomposition of calcium hydroxide: a universal kinetic approach to a physico-geometrical consecutive reaction in solid–gas systems under different partial pressures of product gas. Phys Chem Chem Phys. 2019;21:11615–32.
27. Larysa O, Favergeon L, Johannes K, Kuznik F. New kinetic model of the dehydration reaction of magnesium sulfate hexahydrate: application for heat storage. Thermochim Acta. 2020;687:178569.
28. Gil-González E, Perejón A, Sánchez-Jiménez PE, Medina-Carrasco S, Kupčík J, Šubrt J, et al. Crystallization kinetics of nanocrystalline materials by combined X-ray diffraction and differential scanning calorimetry experiments. Cryst Growth Des. 2018;18:3107–16.
29. Luo L, Jin B, Xiao Y, Zhang Q, Chai Z, Huang Q, et al. Study on the isothermal decomposition kinetics and mechanism of nitrocellulose. Polym Test. 2019;75:337–43.
30. Zhang J, Ma P, Zhang X, Wang B, Wu J, Xing X. Isothermal drying kinetics of paddy using thermogravimetric analysis. J Therm Anal Calorim. 2018;134:2359–65.
31. Kelly CA, Hay JN, Turner RP, Jenkins MJ. The effect of a secondary process on the analysis of isothermal crystallisation kinetics by differential scanning calorimetry. Polymers. 2020;12:19.
32. Málek J, Podzemná V, Shánělová J. Crystal growth kinetics in GeS2 glass and viscosity of supercooled liquid. J Phys Chem B. 2021;125:7515–26.
33. Perejón A, Sánchez-Jiménez PE, Gil-González E, Pérez-Maqueda LA, Criado JM. Pyrolysis kinetics of ethylene–propylene (EPM) and ethylene–propylene–diene (EPDM). Polym Degrad Stab. 2013;98:1571–7.
34. Erans M, Manovic V, Anthony EJ. Calcium looping sorbents for CO_2 capture. Appl Energy. 2016;180:722–42.
35. Arcenegui Troya JJ, Moreno V, Sanchez-Jiménez PE, Perejón A, Valverde JM, Pérez-Maqueda LA. Effect of steam injection during carbonation on the multicyclic performance of limestone ($CaCO_3$) under different calcium looping conditions: a comparative study. ACS Sustain Chem Eng. 2022;10:850–9.
36. Criado JM, González M, Málek J, Ortega A. The effect of the CO_2 pressure on the thermal decomposition kinetics of calcium carbonate. Thermochim Acta. 1995;254:121–7.
37. Rodriguez-Navarro C, Ruiz-Agudo E, Luque A, Rodriguez-Navarro AB, Ortega-Huertas M. Thermal decomposition of calcite: Mechanisms of formation and textural evolution of CaO nanocrystals. Am Mineral. 2009;94:578–93.
38. Maitra S, Chakrabarty N, Pramanik J. Decomposition kinetics of alkaline earth carbonates by integral approximation method. Ceramica. 2008;54:268–72.
39. Perrin F-X, Nguyen TMH, Vernet J-L. Kinetic analysis of isothermal and nonisothermal epoxy-amine cures by model-free isoconversional methods. Macromol Chem Phys. 2007;208:718–29.
40. Sbirrazzuoli N, Vyazovkin S, Mititelu A, Sladic C, Vincent L. A study of epoxy-amine cure kinetics by combining isoconversional analysis with temperature modulated DSC and dynamic rheometry. Macromol Chem Phys. 2003;204:1815–21.